Experimental Characterization of Composite Printed Materials for the Production of Multirotor UAV Airframe Parts

Tomislav Šančić , Marino Brčić , Denis Kotarski * , Andrzej Łukaszewicz *

Posted Date: 28 June 2023

doi: 10.20944/preprints202306.1978.v1

Keywords: UAV; additive manufacturing; material experimental characterization; multirotor UAV airframe; CAx; CAD

Article

Experimental Characterization of Composite Printed Materials for the Production of Multirotor UAV Airframe Parts

Tomislav Šančić [1], Marino Brčić [2], Denis Kotarski [1,*] and Andrzej Łukaszewicz [3,*]

[1] Department of Mechanical Engineering, Karlovac University of Applied Sciences, 47000 Karlovac, Croatia; tomislav.sancic@vuka.hr
[2] Department of Engineering Mechanics, Faculty of Engineering, University of Rijeka, 51000 Rijeka, Croatia; marino.brcic@riteh.hr
[3] Institute of Mechanical Engineering, Faculty of Mechanical Engineering, Bialystok University of Technology, 15-351 Bialystok, Poland; a.lukaszewicz@pb.edu.pl
* Correspondence: denis.kotarski@vuka.hr, a.lukaszewicz@pb.edu.pl

Abstract: In this paper, the characterization of 3D printed materials that are considered in the design of multirotor unmanned aerial vehicles (UAVs) for specialised purposes was carried out. The multirotor UAV system is briefly described, primarily from the aspect of system dynamics, considering that the airframe parts connect the UAV components, including the propulsion configuration, into a functional assembly. Three additive manufacturing (AM) technologies were discussed, and a brief overview was given of selective laser sintering (SLS), fused deposition modeling (FDM), and continuous fiber fabrication (CFF). Using hardware and related software, 12 series of specimens were produced which were experimentally tested utilizing a quasi-static uniaxial tensile test. The results of the experimental tests are given graphically with displacement-force characteristics. In this work, the focus is on CFF technology and the testing of materials that will be used in the production of mechanically loaded airframe parts of multirotor UAVs. Furthermore, an overview was given in such a way that the specimens were grouped, and the mean values of the maximum stress were presented, so that the tested materials could be more easily compared with conventional materials, such as aluminum alloys.

Keywords: multirotor UAV airframe parts; additive manufacturing; continuous fiber fabrication; fiberglass reinforcement; material experimental characterization; uniaxial tensile test

1. Introduction

Technologies of rapid prototyping enabled a great step forward in the development of mechatronic systems, including Unmanned Aerial Vehicles (UAVs). Nowadays, there are numerous types of research and applications of aircraft in various sectors such as aerial photography [1], surveillance [2], precision agriculture [3,4], transport and logistics [5], research [6,7], and many others. Due to the possibility of vertical take-off and landing (VTOL), and therefore stationary flight and moderate-speed flight, multirotor UAVs are suitable for missions that require a high degree of system autonomy. Furthermore, the performance of the propulsion system consisting of several rotors enables greater agility and maneuverability, which consequently enables precise and complex movements. That fact places them in the category of aerial robotic systems and in general for specialised purposes. Major manufacturers mostly offer conventional multirotor configurations that are intended for specific applications. For example, the largest multirotor UAV manufacturer DJI has several aircraft sizes that are intended for aerial photography, from the Mini to the Inspire UAV. In addition, there is a series of Agras UAVs that are intended for smart spraying tasks. These are large series of aircraft for which the frame parts are produced by conventional technologies, such as injection molding.

The multirotor type of UAV is used in more and more specific applications, and small series or unique aircraft are often required. The development of rapid prototyping technology is correlated with the development of specialised multirotor UAVs, where the key area is Additive Manufacturing (AM), so-called 3D printing. There are many studies describing UAV systems that are built using additive technologies, such as fixed-wing type of UAV [8] or considered multirotor [9]. With today's dynamic market demands based on shorter product life cycles that require smaller production batches, there is a need to move from traditional production systems to next-generation production systems [10]. Such systems must have high flexibility and reconfigurability in order to adapt to changes in the market, and this is exactly what is achieved with reconfigurable production systems (RMS) [11]. This is made possible by a quick response to the customer's needs by making products according to his requirements, which achieves his satisfaction. In contrast to the mass customization paradigm [12], where customers choose a product from a multitude of offered combinations, with mass individualization, the customer himself participates in the design of the product, which is suitable for the use of AM technologies, which gives advantages from the economic side due to the creation of a unique product adapted to an individual customer [13]. Increasing demands for unique customer-oriented products switch to the mass individualization paradigm, where the goal is to reduce the price of products to the level of products made by the mass customization paradigm.

AM technologies play a crucial role in the fourth industrial revolution by offering the ability to surpass the limitations of traditional production systems. Due to its flexibility, agility, and speed of placing new products on the market, AM is no longer used only for the creation of prototypes, but also for the serial production of functional structural parts with the required accuracy and mechanical properties. With the development of new materials and forms of workpieces that ultimately lead to an increase in product quality, AM is used more and more often in research, especially in mechatronics, where production can be roughly divided into the design phase and the production phase itself. With this common approach, parts, or 3D objects, are created with the addition of materials, using technology by adding layers on top of each other. There are different AM technologies such as Fused Deposition Modeling (FDM) [14], Stereolithography (SLA) [15], Selective Laser Sintering (SLS) [16], polyjet technology [17], Laminated Object Manufacturing (LOM) [18], and others. Compared to other methods, FDM technology has its advantages, such as the variety of low-cost materials, which is why it is the most commonly used method, but there are always problems related to mechanical properties and dimensional accuracy. The most commonly used conventional materials are acrylonitrile butadiene styrene (ABS), polylactic acid (PLA), and polyethylene terephthalate glycol (PETG).

Additively manufactured polymers alongside polymer composites represent anisotropic materials [19]. With regard to the considered application of the parts, it is extremely important to identify the mechanical properties concerning the material and production parameters. In the research [20], the applicability of test methods for the mechanical characterization of test samples manufactured with FDM technology was discussed. Furthermore, the numerical and experimental study of the PLA material compression uniaxial properties is presented in the research [21]. There are many types of research and works on the topic of improving the mechanical properties of materials that are made with FDM technology. One of the directions is joining plastic with composite materials that are widely used in research and the aerospace industry, where various types of materials and different purposes are represented, such as prototyping and production of wing structures shown in the papers [22,23]. The paper [24], gives an overview of strategies such as short fiber reinforcement (SFR), continuous fiber reinforcement (CFR), powder addition reinforcement (PAR), and other methods. Further related to the production of UAV parts, in paper [25] a novel sandwich structure consisting of an ABS base laminated with carbon fiber reinforced polymer (CFRP) layers was proposed. The main disadvantage of such materials is the time required to manufacture such parts. The solution is imposed with new 3D printers that are based on FDM technology, known as continuous fiber fabrication (CFF). In the paper [26], an experimental investigation of the additive manufacturing of continuous carbon fiber composites was carried out.

Preprints (www.preprints.org) | NOT PEER-REVIEWED | Posted: 28 June 2023 doi:10.20944/preprints202306.1978.v1

In this paper, conventional and composite materials for 3D printing are experimentally tested and compared. A multirotor type of UAV for specialised purposes is studied, and considering the need for making prototypes or small series of aircraft, AM technologies are investigated for the production of airframe parts, especially structural parts that are mechanically loaded. In order to construct the aircraft assembly more efficiently, the process of characterizing the materials of the airframe parts was integrated into the design process. Twelve series of test specimens were produced using three AM technologies (FDM, SLS, CFF) and the samples were mechanically tested. As an orientation value and comparison, aluminum alloys will be used due to their large share in mass production with high-reliability requirements in the automotive industry, which is crucial when designing a multirotor UAV. Test results and characterization of the considered materials are presented and discussed.

2. Multirotor UAV System Description

Multirotor type of UAVs represents an extremely complex system in terms of design and control. Such a type of aircraft is an inherently unstable system, which results from the fact that it cannot independently return to the point of balance (hover) if it loses the functionality of the control loops, but will fall or begin to move uncontrollably in space. Furthermore, multirotor UAVs are nonlinear systems since rotor aerodynamic forces and moment characteristics are nonlinear functions with respect to angular velocities. The multirotor UAV is mathematically described by a rigid body dynamic model with six second-order differential equations, twelve state variables, and N input variables, which makes them a multivariable system. From the design point of view, it is important to emphasize that such UAVs are high-energy consumption systems, considering that for the needs of motion, rotary wings are used, which with their aerodynamic forces, among other effects, have to cancel the gravity force.

2.1. Preliminary Description of the Multirotor UAV Configuration Dynamics

The number of control variables depends on the aircraft configuration, which is determined by the geometric arrangement of the rotors. Conventional configurations are characterized by a planar arrangement of rotors. Typical designs are configured with four rotors, the so-called quadrotor or quadcopter [27], with six rotors, hexarotor (Figure 1), and with eight rotors (octorotor). Aircraft dynamics, which is influenced by the forces and moments of the environment, and of the aircraft propulsion subsystem, is described by the following equation

$$\dot{\boldsymbol{\nu}} = \mathbf{M}_{\mathrm{B}}{}^{-1}(-\mathbf{C}_{\mathrm{B}}(\boldsymbol{\nu})\boldsymbol{\nu} + \mathbf{g}_{\mathrm{B}} + \mathbf{d} + \mathbf{u}_{\mathrm{B}}), \tag{1}$$

where $\dot{\boldsymbol{\nu}}$ is the acceleration vector with respect to the coordinate system which is attached to the aircraft body assuming that the origin coincides with the center of gravity, while the coordinate system axes coincide with the aircraft's main axes of inertia. The equations of motion were derived using the Newton-Euler method whereby $\mathbf{M}_{\mathrm{B}}$ is a rigid body inertia matrix defined with mass and inertia moments. Given that the rigid body rotates, $\mathbf{C}_{\mathrm{B}}(\boldsymbol{\nu})$ represents the Coriolis and centripetal matrix that describes the inertial forces and moments. The gravitational force vector $\mathbf{g}_{\mathrm{B}}$ can be precisely described considering that the gravitational force acts in the vertical axis of the coordinate system which is fixed in the base station. External disturbances such as wind gusts, and unmodeled dynamics such as the gyroscopic effect make up the total disturbance vector $\mathbf{d}$.

The only vector through which the dynamics of the aircraft can be directly influenced is the control vector $\mathbf{u}_{\mathrm{B}} = [f_{\mathrm{X}} \quad f_{\mathrm{Y}} \quad f_{\mathrm{Z}} \quad \tau_{\phi} \quad \tau_{\theta} \quad \tau_{\psi}]^{\mathrm{T}}$, containing forces $\mathbf{f} = [f_{\mathrm{X}} \quad f_{\mathrm{Y}} \quad f_{\mathrm{Z}}]^{\mathrm{T}}$ and moments $\boldsymbol{\tau} = [\tau_{\phi} \quad \tau_{\theta} \quad \tau_{\psi}]^{\mathrm{T}}$ of the propulsion configuration (subsystem, module). It is given by the following expression

$$\mathbf{u}_{\mathrm{B}} = \boldsymbol{\Gamma}_{\mathrm{B}}\boldsymbol{\Omega}, \tag{2}$$

where $\boldsymbol{\Gamma}_{\mathrm{B}}$ is a control allocation matrix that describes the propulsion configuration of the multirotor UAV, which is defined by the geometric arrangement and characteristics of the rotor. The configuration geometric arrangement is defined by the position and orientation of each rotor in

Preprints (www.preprints.org) | NOT PEER-REVIEWED | Posted: 28 June 2023 doi:10.20944/preprints202306.1978.v1

relation to the aircraft coordinate system, and a more detailed derivation is presented in the previous research [9,28]. In conventional propulsion configurations, the rotors are electric propulsion units (EPUs) whose central part is the brushless DC (BLDC) motor driven by electronic speed controller (ESC). This type of electric propulsion converts electrical energy, obtained from Lithium-Polymer (LiPo) batteries, into mechanical work. Fixed-pitch propellers mounted on the rotor axis of the BLDC motor, with their rotation, create aerodynamic effects, from which it follows that the aircraft dynamics directly depend on the rotors' angular velocities. It is assumed stiffness of the propeller and that the aerodynamic effects of each rotor consist of thrust force which can be modeled as $f_{\mathrm{R}_i} = k_{\mathrm{f}}{\omega_i}^2$, and drag torque $\tau_{\mathrm{R}_i} = k_{\tau}{\omega_i}^2$. From these relations, it follows that $\boldsymbol{\Omega} = [{\omega_1}^2\ {\omega_2}^2\ \ldots\ {\omega_{\mathrm{N}}}^2]^{\mathrm{T}}$ is the vector of the square of the rotors angular velocities. Figure 2 shows the characteristics of the EPU based on the Tiger motor U13 II [29], which is intended for usage in so-called heavy-lift multirotors. The data shown on the graph were obtained by carrying out experimental measurements and using an approach to the characterization of EPU units that was presented in the previous research [28].

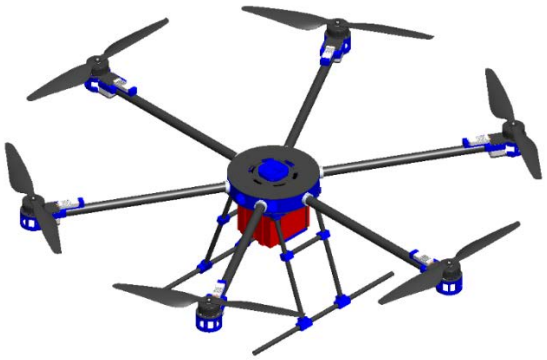

Figure 1. Multirotor UAV platform 3D model.

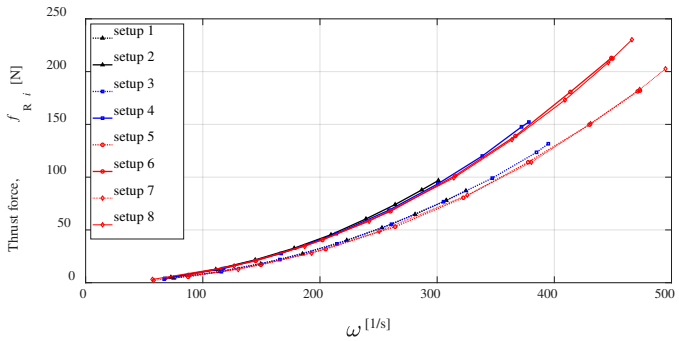

Figure 2. Thrust force as a function of rotor angular velocity [26].

2.1. Specialised Multirotor UAV Design Considerations

When it comes to the design of specialized multirotor UAVs, such aircraft are produced in small series and often exist as unique systems designed to perform specific tasks. Unlike commercially available aircraft produced in large series, in small series production, the price per unit increases dramatically. In that case, it is important to consider technologies for rapid prototyping where manufacturing costs are not sensitive to changes in production volume. In general, it can be said that the design of the aircraft system primarily depends on the purpose, that is, the profile of the mission that the aircraft typically needs to perform. The aircraft system can be divided into four key subsystems, where from the aspect of designing and mass budgeting, each subsystem is defined by its mass. Payload equipment and cargo are determined by the purpose of the aircraft and further dictate the choice of parameters and components of the control, propulsion, and energy subsystem.

Preprints (www.preprints.org) | NOT PEER-REVIEWED | Posted: 28 June 2023 doi:10.20944/preprints202306.1978.v1

Given that the payload mass m_{PL} is actually fixed by the selection of the necessary components and parts of the assembly, and furthermore the mass of the control subsystem (avionics) m_{AV}, which also includes the sensors necessary to perform the mission, the design is actually reduced to the selection of the propulsion and energy subsystem parameters, which determines the propulsion m_{PM}, and energy subsystem mass m_{EM}. The total mass of the aircraft obtained by adding the masses of the subsystems represents the take-off mass of the aircraft and is given by the following expression

$$m = m_{\mathrm{PL}} + m_{\mathrm{EM}} + m_{\mathrm{PM}} + m_{\mathrm{AV}}. \quad (3)$$

The basic performance of the aircraft is defined by the ratio of the maximum thrust of the propulsion subsystem in the vertical aircraft axis and the take-off mass. The unwritten rule is that this so-called thrust-to-mass ratio (TMR) is approximately two, except in extreme situations such as racing drones, and a more precise ratio can commonly be read from the specifications of the propulsion components manufacturers. As mentioned earlier, multirotor UAVs are characterized by high energy consumption, which in turn depends on the aircraft's mass. When designing a system, the ratio of battery mass and capacity is one of the key data. The propulsion and energy subsystems are mutually dependent because, for example, as the power of the aircraft increases, so does the need for energy, which results in a larger mass of the aircraft. The design of the propulsion subsystem is the most complex part of the overall design in terms of the mechanical properties that the parts of the assembly should possess. The multirotor type of UAV can be used in a wide power range, from several tens of watts to several tens of kilowatts, so it is necessary to choose materials and technologies concerning the selected propulsion components. In the aircraft design phase, the parts of the frame that connect everything into a functional assembly have to be modeled and manufactured based on the selected components, where the main requirements are high strength and absorption energy, and low specific mass (weight).

The production of parts for specialised multirotor UAVs can be divided into two main phases. The first phase represents the phase of designing the aircraft where various CAx techniques and tools are utilized, which are outlined through previous research [30–32]. In this phase, parts and assemblies are modeled using a 3D software package, and also simulations of airframe parts that need to meet certain mechanical properties can be carried out. The final versions of the 3D CAD model are exported performing a triangulation process to STL format, which is further used for the production of parts. In this research, the SOLIDWORKS software package is used for 3D modeling purposes. The next phase is the production, i.e. prototyping of the frame parts. The first step of the prototyping phase is setting print parameters in accordance with the selected AM technology. The print parameters are adjusted in the software package, the so-called slicer, which actually makes up the software package of a particular 3D printer. After setting the parameters, the g-code is generated for the 3D printing execution, with which the 3D printer creates a physical model. The last step in this phase is the post-processing of the parts, such as removing the support, or sandblasting and cleaning the parts produced by the SLS technology.

3. Additive Manufacturing Considerations and Experimental Testing

Given that multirotor UAVs are used in various applications where small series or prototype aircraft are used, it is important to consider rapid prototyping technologies in the system design phase. This is an additional benefit from the aspect of using such aircraft in engineering education and research. In addition to the fact that for small series rapid prototyping technologies are cheaper compared to conventional technologies, they also significantly reduce development time through rapid iteration and the possibility of early and frequent testing of many different designs or partial designs with critical features. The development of AM and new materials lead to an increase in the quality of the product, it is used more and more often in various industries such as biomedicine, the automotive industry, and the space industry [33]. AM technology enables the production of structural parts with the required accuracy and mechanical properties at increased production speed, given that the development procedure is relatively simple for different technologies.

Preprints (www.preprints.org) | NOT PEER-REVIEWED | Posted: 28 June 2023 doi:10.20944/preprints202306.1978.v1

3.1. Considered Additive Manufacturing Technologies

In the field of making UAVs that are used mainly for research or education, FDM 3D printing technology is mainly used, and recently, due to the availability of cheaper equipment and materials, SLS technology is prominent. In this paper, specimens made with SLS technology using the Lisa 3D printer by Sinterit, and using Sinterit Studio software, were investigated. For the considered FDM technology, a series of samples made on a low-cost Prusa i3 MK3s 3D printer will be tested using the corresponding Prusa Slicer software. For UAVs that are mechanically loaded, parts made of composite materials are used, most often carbon fiber tubes and plates, from which structural parts can be quickly made. This means that it takes relatively little time from the design phase to the production of the aircraft, which is why it is cheaper. Although 3D printing is widely used, it is mostly for smaller aircraft. For aircraft with a large payload, it is necessary to design parts that are mechanically more loaded, and most often the propulsion airframe parts are made by processing aluminum. The development of CFF 3D printing technology enabled the production of parts made of plastic-reinforced materials whose mechanical properties can be compared to aluminum parts, especially in combination with composite parts. In this work, the emphasis is on testing the samples that were produced by CFF technology, where the Onyx Pro 3D printer by Markforged is utilized.

Regardless of the type of AM technology, the production of the structural part is based on layer-by-layer construction, which is also the case with SLS technology. This AM technology uses powder materials that are sintered by thermal energy generated by a laser. Modeling by this process can be applied to all materials with powder particles that are sintered due to the application of heat. The first and most commonly used powder materials in this technology are polymer materials, the most important of which are polycarbonate (PC) and polyamide (PA). To further improve the mechanical and thermal properties of the material, reinforced polymers are used, where fiber reinforced is added to PA materials. Furthermore, this technology enables the production of metal and ceramic parts. Unlike other technologies that belong to rapid prototyping, SLS technology is suitable for the production of small series of parts with complex geometry.

A schematic representation of the working principle is shown in Figure 3, where the manufacturing process begins with the creation of a laser beam that is directed by the laser system to the exact desired position on the XY plane of the printed part. Changing the height of the layer is most often performed by lowering the build platform, the so-called bed placed in the manufacturing chamber. After the layer has been formed, the powdered material needed to create a new layer is added from the material feed chamber via a roller. The process of making the layer starts as a result of the action of the laser beam into the powder material due to the heat action of the powder particles tend to fuse or sinter. The required temperature applied to the powder particle must be very high within certain limits, i.e. it must be between the crystallization temperature and the melting temperature of the particle [34]. In this research, test specimens were made from polyamide material with the trade name PA12, using Sinterit Lisa Pro 3D printer Sinterit Studio software.

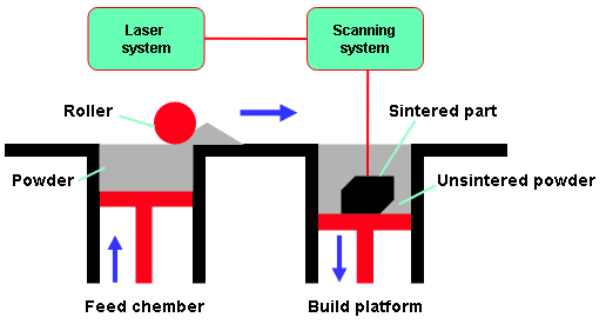

Figure 3. SLS technology - schematic overview.

FDM 3D printing technology is the most popular and most frequently used technology in research and development, education, and industry. It is based on the melting of solid polymer

Preprints (www.preprints.org) | NOT PEER-REVIEWED | Posted: 28 June 2023 doi:10.20944/preprints202306.1978.v1

materials into a semiliquid that passes through a nozzle, forming objects by applying the polymer layer by layer. The created objects are made of thin layers of material whose direction of application defines the mechanical properties of the anisotropic material. Since it is applied layer by layer, the support material is printed for parts with overhanging geometries [35]. Compared to other AM technologies, FDM has its advantages, such as the variety of products and low material costs, which is why it is the most widely used. On the other side, there are still problems related to mechanical properties, dimensional accuracy, consistency, and undetected defects within the structure of the products. The most commonly used thermoplastic materials for FDM technology are ABS, PLA, and PETG. The working principle of FDM technology is schematically represented in Figure 4. Test specimens were made from PLA and PETG materials, using a Prusa i3 mk3 3D printer and Prusa slicer. Furthermore, using Markforged equipment and a slicer, test specimens were also made using FDM technology from micro carbon fiber filled nylon material, commercial name Onyx.

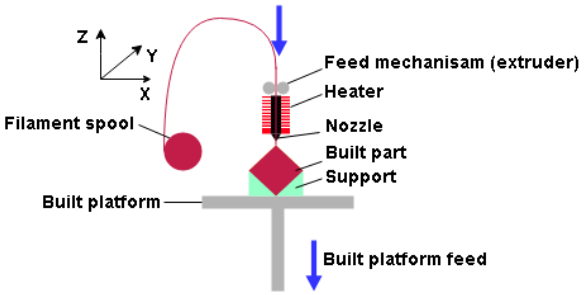

Figure 4. FDM technology - schematic overview.

The main disadvantages of 3D printed models using the FDM technology are low mechanical properties. Due to the FDM working principle, by adapting this technology it is possible to produce parts that are reinforced with composites. Considering the type of composite with which the polymer material is reinforced, they can be divided into fiber reinforcements, particle reinforcements, and nanoparticle reinforcements. Composite materials are usually synthetic carbon fiber (CF), glass fiber (GF), and kevlar fiber with significantly high tensile properties. Additionally, more environmentally friendly natural biodegradable fibers can be produced [36]. The addition of fibers as part of the reinforced polymer objects can be performed with one nozzle to print the matrix material and the reinforcement material, as shown in Figure 5b. A composite structure model is obtained by strengthening the thermoplastic matrix where the fibers and the matrix are mixed before injection. Polymer materials with a reinforced matrix, have significantly increased strength and are used more and more, considering that at the same time they have a smaller mass [37].

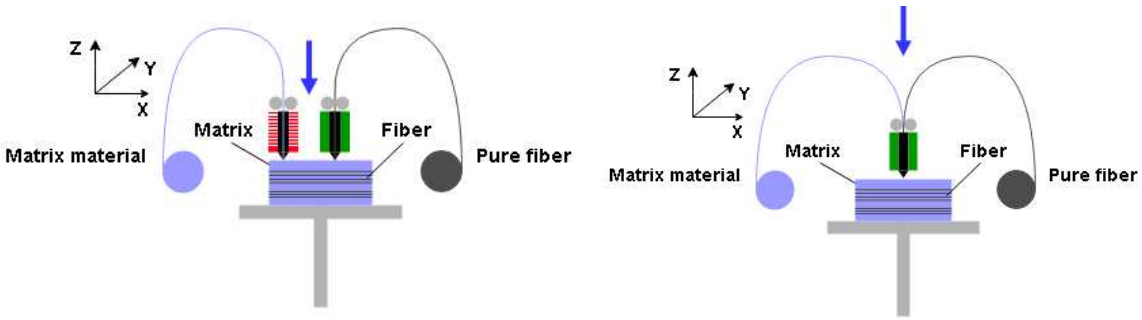

(**a**) (**b**)

Figure 5. CFF technology - schematic overview: (**a**) Separate nozzles; (**b**) One nozzle.

In this paper, the CFF technology with direct reinforcement is discussed, which requires two nozzles, one for the matrix material and the other for the reinforcement fibers, where a composite sandwich structure is formed, as schematically shown in Figure 5a. On the Onyx Pro printer, this

Preprints (www.preprints.org) | NOT PEER-REVIEWED | Posted: 28 June 2023 doi:10.20944/preprints202306.1978.v1

system of separate nozzles is used to produce parts of the sandwich structure of the composite, where the Onyx material is used as the matrix and the fiberglass as reinforcement. The mechanical properties of the parts depend on parameters that can be adjusted, such as the number of reinforcement layers and the different geometric arrangements of fibers. Models made with CFF technology have an advantage over those made with conventional FDM technology in terms of significantly higher tensile strength depending on the proportion of fibers in the composite structure. Test specimens with a different number of reinforcement layers and with various fiber orientations were considered in the testing phase.

3.2. Experimental Methods and Equipment

Although numerous methods have been used so far to test the mechanical properties of printed materials such as the Charpy test [38] or rotating bending fatigue analysis [39], uniaxial tensile testing was further investigated. Test specimens according to the ISO 527-2 standard (Figure 6), with a square cross-section, were modeled in the Solidworks software package, then exported in .stl format suitable for 3D printing. The print orientation of the test specimens placed on the XY plane of the 3D printer is shown in Figure 6.

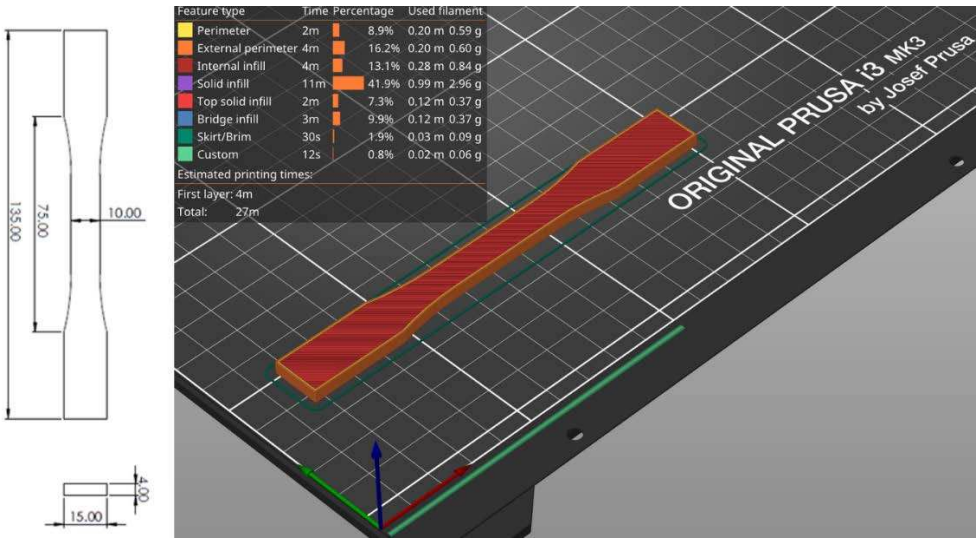

Figure 6. Test specimen (ISO 527-2 standard test specimen for uniaxial quasi-static tensile testing) – g-code generation in a slicer.

Researching the literature has determined that the print orientation where the direction of the layers is perpendicular to the direction of the test force, gives the lowest values of tensile strength due to simple delamination of the layers. For this reason, such an orientation of the test specimens will not be examined. The data described by the 3D CAD model, according to which the test specimen is made, is inserted into the software called slicer, which is the link between the real and digital model in such a way that the steps and movements that the printer will perform during the creation of the 3D model are described by G code. The generated G code is transferred to the printers where the manufacturing begins.

The test specimens were subjected to a quasi-static uniaxial tensile test on a Shimadzu AG-X plus universal industrial equipment (Figure 7), which can achieve a tensile test force of up to 100 kN. The test was carried out at a constant speed of 30 mm/min, without the use of external stress reading devices. The accompanying software of the equipment creates a stress-strain diagram from which the mechanical properties of the material and the critical points of the stress-strain diagram can be analyzed. Raw data measured over a certain time interval during the test are suitable for interpretation in the MS Excel or Matlab software package. During the testing of polymer materials, clamping problems occur. Due to the lower tensile and compressive strength of the sample, it is not possible to clamp the specimens into packs with the same force as aluminum and steel specimens,

Preprints (www.preprints.org) | NOT PEER-REVIEWED | Posted: 28 June 2023 doi:10.20944/preprints202306.1978.v1

because during the test specimen breaks in a place that is not intended for it. These problems are especially pronounced when clamping composite test specimens because the highest values of tensile and compressive strength are expressed in the direction of the fibers, so such values should be achieved in the direction of the test axis, which is perpendicular to the forces that act when clamping the specimens. For this reason, by increasing the tensile strength of the composite specimen, a slip can occur between the packs and the clamped specimen.

Figure 7. Experimental equipment: (**a**) SHIMADZU AG-X; (**b**) performing quasi-static uniaxial tensile stress on the test specimen.

3.3. Selection of Test Specimens Technological Parameters

In addition to striving to achieve the highest possible tensile strength of the tested specimens, it is more important to express the limit of elasticity. Due to the very small differences between the elastic limit and the maximum tensile strength of the printed samples, the maximum tensile strength is used as an orientation value for testing purposes. The construction of unmanned aerial vehicles must ensure sufficient tensile strength and criteria of rigidity and stability. In order for the aircraft to be in a functional state, its structural parts must remain in the elastic region, that is, there must be no permanent deformations in the plastic region that would cause displacements of the structure that could adversely affect flight dynamics. The forces that occur due to thrust during flight would deform ductile materials, so it is desirable to have as much rigidity as possible in the construction material. To test the mechanical properties of airframe parts that are statically loaded with the load carried by aircraft, the best description is given by the uniaxial static tensile test that was carried out in this research. The criteria that the material must meet are low mass, high stiffness, maximum elasticity limit, and orientation of composite fibers that will be satisfactory in different directions of force.

For this reason, a uniaxial quasi-static tensile test is performed on standard test specimens, from which a force-displacement diagram is obtained. During production, layer by layer, the anisotropic property of the material occurs, due to the dimensional inaccuracy of the production, inhomogeneity also occurs, which results in different mechanical properties of the material and is present in all printing technologies, unlike mold-injected parts. This is why it is necessary to test several AM technologies using different materials and 3D printing parameters. Five test specimens are produced for each specimen series (S01 – S12). Low-cost PLA and PETG materials were considered, from which specimens (S01 – S06) are produced by FDM technology using Prusa equipment and a slicer. Standard printing parameters were investigated, and furthermore, the infill percentage and the number of edge layers were varied. Table 1 shows the materials and parameters of 3D printing for test specimens manufactured using FDM technology. The test specimens (S01 - S06) have four floor layers, six roof layers, and a triangles infill pattern. To make a test specimen (S07) with SLS technology, the factory parameters set in Sinterit Studio software are used, and the test specimens are made of PA12 material.

Table 1. FDM print parameters.

Preprints (www.preprints.org) | NOT PEER-REVIEWED | Posted: 28 June 2023 doi:10.20944/preprints202306.1978.v1

The stiffness of the non-composite polymer materials used in the tests made by FDM and SLS

Specimen series	Material	Infill %	Wall layer number (vertical shells)	Mass [g]	Time [min]
S01	PLA	20	2	5.90	27
S02	PLA	40	2	6.62	30
S03	PLA	20	4	6.34	29
S04	PETG	20	2	6.04	27
S05	PETG	40	2	6.78	30
S06	PETG	20	4	6.50	29

technology is sufficient for the production of parts of UAVs, while their strength is low for the production of functional structural airframe parts such as parts of the UAV propulsion assembly. The goal is to achieve the highest possible strength of the test specimens compared to conventional FDM and SLS technologies and to be comparable to aluminum alloys. Due to the most similar conditions when UAVs hit the ground or other unpredictable objects, a car chassis is compared as a reference, where it is tried to achieve a tensile strength equal to or greater than the aluminum alloys used for the production of structural car chassis. This is made possible by CFF 3D printing technology, where composite specimens are obtained by combining matrix and reinforcement materials. Then micro carbon fiber-filled nylon matrix material is investigated, from which test specimens (S08) with factory parameters (triangular infill 37%) are produced by Markforged Onyx 3D printer. Reinforcement materials are made from different fiber orientations with the aim of achieving the required values for the design of UAVs. The considered 3D printing parameters of composite materials are shown in Table 2.

Table 2. CFF print parameters.

Specimen series	Material	Number of reinforcement layers / Fill type	Fibre reinforcement angles	Mass [g]	Time [min]
S08	carbon fiber filled nylon	None	-	6.14	33
S09	carbon fiber filled nylon + fiberglass reinforcement	8 / Concentric	-	6.24	68
S10	carbon fiber filled nylon + fiberglass reinforcement	8 / Isotropic	$[0/90/\pm45]_8$	6.95	80
S11	carbon fiber filled nylon + fiberglass reinforcement	8 / Isotropic	$[30/45/60/0]_8$	6.95	82
S12	carbon fiber filled nylon + fiberglass reinforcement	12 / Isotropic	$[30/45/60/0]_{12}$	7.52	92

The mechanical properties depend on the number of reinforcement layers, as well as the reinforcement fill type. Changes in mechanical properties with a change in the proportion of fibers in printed composites with fiberglass reinforcement are noted in the paper [40]. The initial sample consisted of four layers of fiberglass with a total volume share of approximately 4%, so for subsequent samples, 4 layers were added up to 30 layers of fiberglass (33% volume share). They did not reach the limit of 40% to 50% fiber content in CFF, however, it was clearly proven that with each increase in the fiber content, the maximum tensile strength of the tested sample increases. The arrangement of fibers can be divided into concentric, which is shown in Figure 8, and isotropic. The concentric fiber pattern orientation has fibers in the directions as the walls in the FDM process following the

Preprints (www.preprints.org) | NOT PEER-REVIEWED | Posted: 28 June 2023 doi:10.20944/preprints202306.1978.v1

wall of the model, and for that pattern, a series (S09) of test specimens were 3D printed according to standard Markforged parameters. Isotropic fiber orientation represents parallel fiber lines at different angles. Other test specimen series with different numbers and fiber orientations were made using this pattern approach.

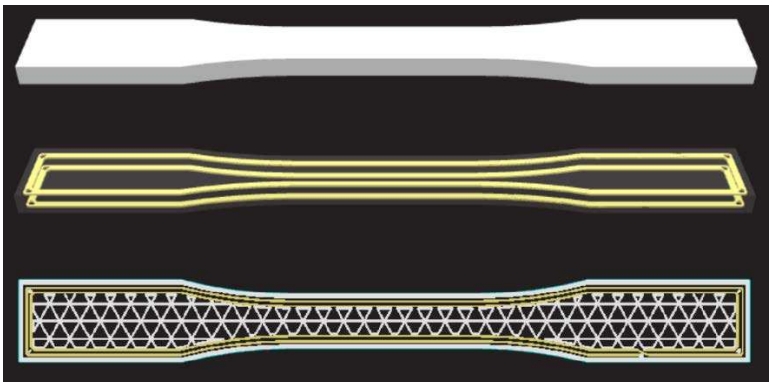

Figure 8. S09 test specimen with concentric fiber reinforcement.

Fibers in the axial direction have very high strength, but also composites with the action of force perpendicular to the direction of the fiber have the lowest strength, which is why it is necessary to make a compromise with the orientation of the fibers because in reality there are multiaxial forces acting on the structure. Placing the fibers longitudinally at 0 degrees in the load direction gives the highest tensile strength. By rotating the fibers (increasing the angles), the tensile strength of the composite material decreases, because the applied force is no longer only longitudinal to the fibers but also to the layers of the matrix. By increasing the angles from 0° to 90°, more and more load is transferred to the matrix, which has a significantly lower tensile strength than the fibers, and thus the overall tensile strength of the composite material decreases. In the research [41] such behavior of the material was shown, where the orientation of the fibers was varied by increasing the angle by 22.5° from 0° to 90°. When constructing the airframe of UAVs, the bending load on the rotor arms caused by the thrust of the propeller has a great influence on the airframe construction. When making such parts from composite structures, it is essential to take into account the anisotropic properties of CFF specimens that, due to bending, cause variations in the strain rate, increasing the shear stress between layers that lead to material failure [42]. The behavior of the flexural properties by testing the material is described in the work [43], where increasing the angle of the fibers increased the ductility of the tested specimens. With the structure of the specimens with angles [+45°/-45°], they could not break due to high ductility, however, by adding more layers, a more balanced structure is obtained [42], which is the reason for testing the orientation [30,45,60,0]. The test is carried out for three different setups (S10 - S12) of isotropic reinforcement parameters, which are shown in Table 2. Figure 9 shows the geometric arrangement of fibers considered in the test.

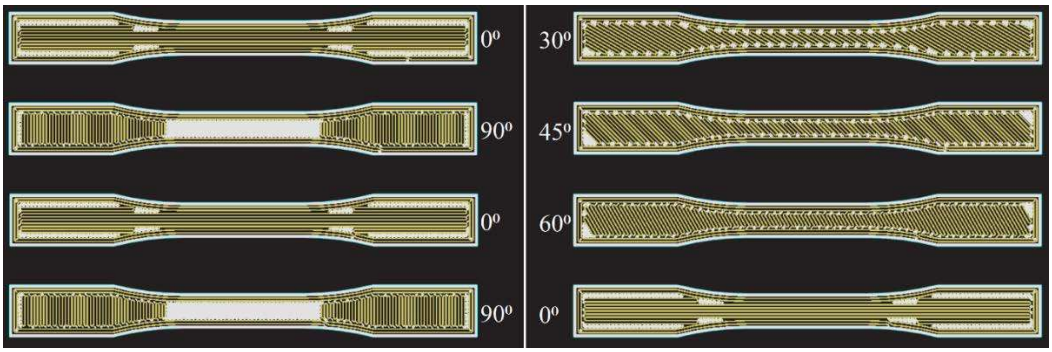

Figure 9. CFF - fibre reinforcement angles.

3.4. Experimetntal Testing Procedure

Preprints (www.preprints.org) | NOT PEER-REVIEWED | Posted: 28 June 2023 doi:10.20944/preprints202306.1978.v1

Technological parameters of test specimens are adjusted for certain technologies in software tools that come with 3D printers. This step is also the first step in the production of the airframe parts that make up the UAV system, and the output of the step is the g-code that is executed on the 3D printer. After adjusting the considered parameters for a particular series of test specimens, it is necessary to prepare the necessary material in the additive manufacturing execution step, which is in the form of filament coils for FDM and CFF technologies, and in powder form for SLS technology. With CFF technology, for the used material, it is necessary to dehumidify the box in which it is placed, and before starting printing, it is necessary to create a purge line of ejected material located between the dry box and the nozzle. With SLS technology, a sieve is used to prepare the material, which is fed into the feed chamber. After the material is ready for production, the g-code execution itself follows. The execution time depends on the technology and the parameters of individual technologies and is shown in Tables 1 and 2 for test specimens. After the end of printing, depending on the technology, the parts need to be post-processed. When printing test specimens, with FDM and CFF technology, there is no post-processing, because due to the geometry of the test specimens and the orientation of the print considered in this research, there are no support structures. With SLS technology, it is necessary to clean the test samples from powder using sandblaster hardware.

When the production step of each series of test specimens is completed, the testing stage is approached, where it is necessary to prepare a test specimen in the clamp of the experimental hardware. After the sample is clamped, the measurement is started for the selected test parameters. During the test, data acquisition is performed and raw data are obtained in the form of vectors. In addition, experimental software generates a report with a graphic display of the test results. In this research, the raw data are further interpreted in the Matlab software package and are graphically presented in the form of a force-displacement diagram. In the next chapter, the test results and characterization for the considered series of samples (S01-S12) are presented. Figure 10 schematically shows the material testing process, the integration of which in the design process enables a more efficient design of structural parts and the aircraft assembly in general. Furthermore, the testing process may include other methods, such as the bending or Charpy impact test.

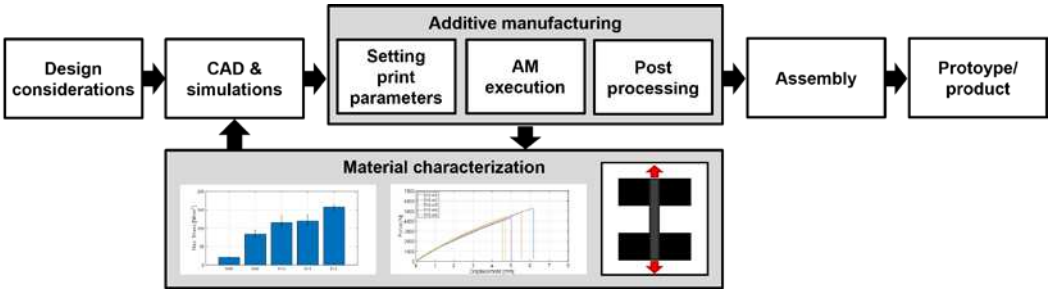

Figure 10. Integrated experimental procedure for material characterization.

4. Results of Experimental Testing

Investigation of the mechanical properties of the printed samples by a uniaxial tensile test is shown by the displacement-force diagrams. For each series of different samples which are shown in Tables 1 and 2, five test specimens were used to obtain more accurate results. Each sample in the series from S01 to S12 is shown separately on the displacement force diagrams.

4.1. Measurement Results Shown by Displacement-Force Diagrams

The first group of materials made by the FDM process consists of samples S01, S02, and S03, which are made of PLA material. The mechanical properties depend on the parameters of the print, and this paper considers the infill (percentage) and the number of vertical shells. The first series of samples use the default settings, in the second series, the percentage of infill has been doubled, while in the third series, the number of vertical shells has been doubled. From the measurement results (Figures 11–13), it can be seen that with an increase in the number of vertical shells, the mechanical

Preprints (www.preprints.org) | NOT PEER-REVIEWED | Posted: 28 June 2023 doi:10.20944/preprints202306.1978.v1

properties improve more significantly in relation to an increase in the percentage of infill, which can further serve as a milestone in the design of airframe parts that will be made by the FDM process from PLA material, which require higher tensile strength. Although slightly, S03 samples are also lighter comparing S02 samples and the printing time is slightly shorter.

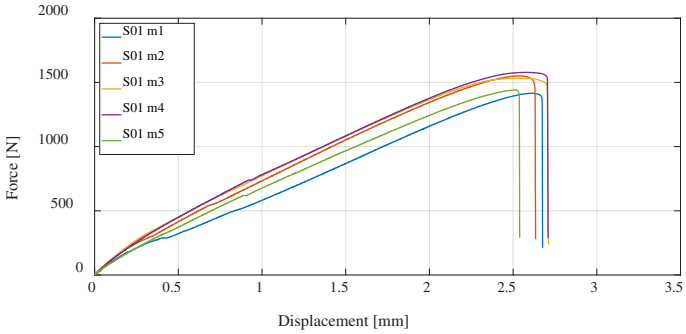

Figure 11. Displacement-force diagram for specimen 1 (S01) series experimental measurements.

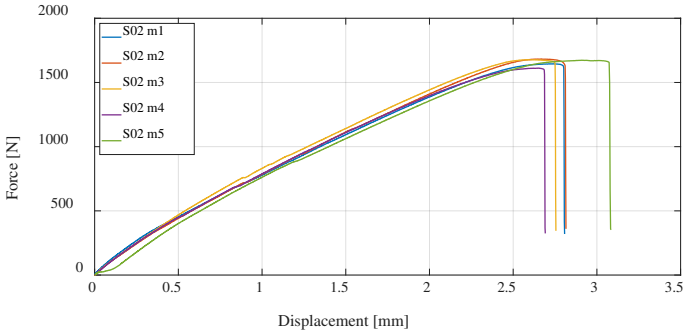

Figure 12. Displacement-force diagram for S02 experimental measurements.

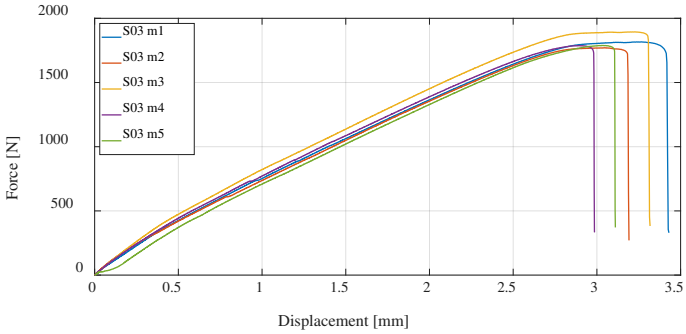

Figure 13. Displacement-force diagram for S03 experimental measurements.

The next three series of test specimens are also produced using the FDM process but from PETG material. The same 3D printing parameters were considered, and as with PLA material, it can be concluded that samples with a higher percentage of infill have higher tensile strength than the default settings, while samples with twice the number of vertical shells have the highest, as shown in Figures 14–16. In relation to PLA material, it is important to emphasize that PETG material generally has lower tensile strength, but is more resistant to elevated temperatures and chemical influences.

Preprints (www.preprints.org) | NOT PEER-REVIEWED | Posted: 28 June 2023 doi:10.20944/preprints202306.1978.v1

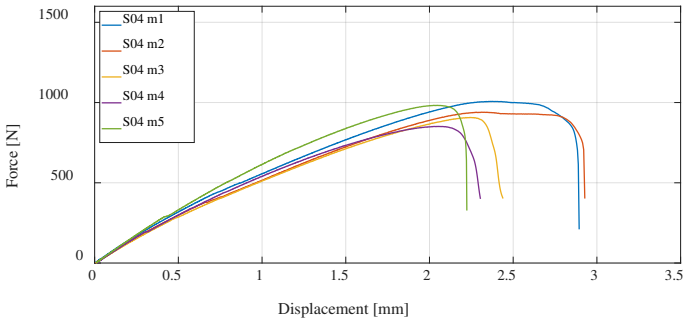

Figure 14. Displacement-force diagram for S04 experimental measurements.

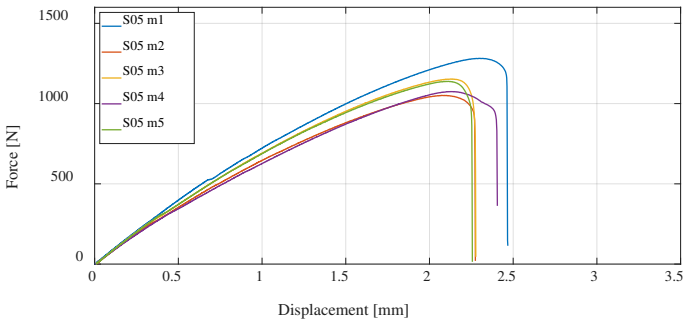

Figure 15. Displacement-force diagram for S05 experimental measurements.

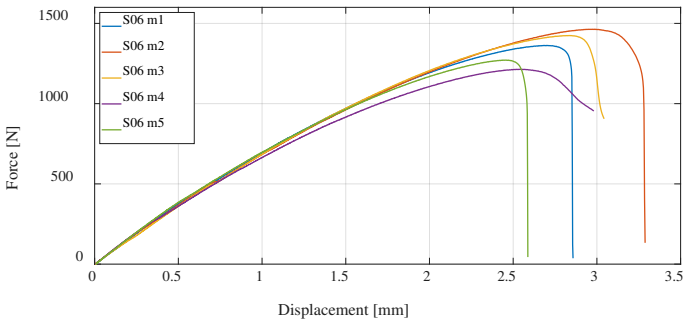

Figure 16. Displacement-force diagram for S06 experimental measurements.

Utilizing the SLS process, one series of test specimens will be made using PA12 powder material. Compared to the test specimens made by the FDM process from PLA and PETG materials, S07 has significantly higher ductility and higher tensile strength. Due to the manufacturing process, a greater homogeneity of the material is obtained compared to the FDM processes, thus there is greater independence of the direction of the force acting on the sample, which is more credible for real structural UAV airframe parts, which are rarely loaded uniaxially. Figure 17 shows the results of the experimental test for S07 specimens.

Preprints (www.preprints.org) | NOT PEER-REVIEWED | Posted: 28 June 2023 doi:10.20944/preprints202306.1978.v1

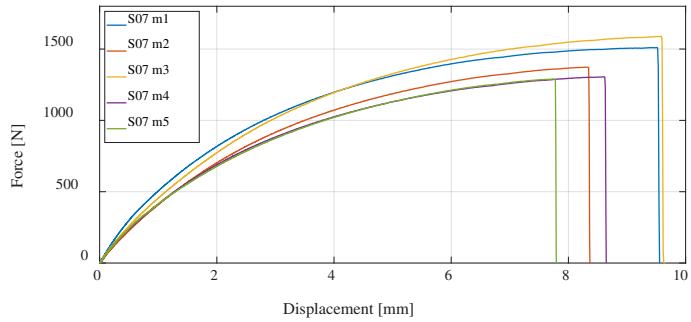

Figure 17. Displacement-force diagram for S07 experimental measurements.

The next series of test specimens will be produced using Markforged equipment and software, which, in addition to the classic FDM process, also enable the production of parts using the CFF process. First, a series of samples made of Onyx carbon fiber filled nylon material, without reinforcement, will be tested. For this material, the highest ductility is obtained, but also the lowest tensile strength. Due to its high ductility, which causes displacement of the test specimen, and tensile strength values close to those of PETG and PLA samples, a significantly larger area under the curve of the graph is obtained, i.e. absorption energy of the specimen. From the point of view of the impact of the UAV on the objects, it is very favorable, however, larger displacements at lower load forces would lead to problems of flight dynamics. Due to its high ductility, this material is suitable for use as a matrix of a composite structure that will be tested further.

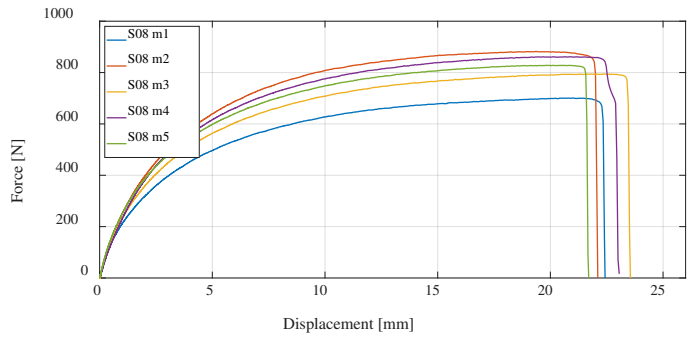

Figure 18. Displacement-force diagram for S08 experimental measurements.

Furthermore, the CFF process will be considered, which enables the production of parts reinforced with fiberglass, which results in reinforced composite materials. Anisotropy of printed parts is present regardless of how the printing parameters are selected in the slicer, however, in the case of composite structures, the printed polymer forms only a material matrix that is equally printed in all layers of the part. The second part of the composite structure, the fiberglass reinforcement, can be oriented differently to each printing layer. In this research, four series of test specimens were considered. The first composite structure of specimens S09 were made by concentric distribution of fibers in a standard test specimen. All other tubes of series S10, S11, and S12 have an isotropic fiber arrangement, with different fiber orientations. As can be expected, the most significant increase in the value of the maximum tensile strength has the samples with an increase in the number of reinforcements or fiberglass.

Preprints (www.preprints.org) | NOT PEER-REVIEWED | Posted: 28 June 2023 doi:10.20944/preprints202306.1978.v1

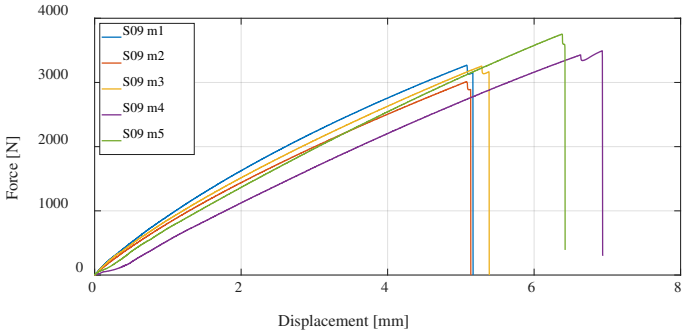

Figure 19. Displacement-force diagram for S09 experimental measurements.

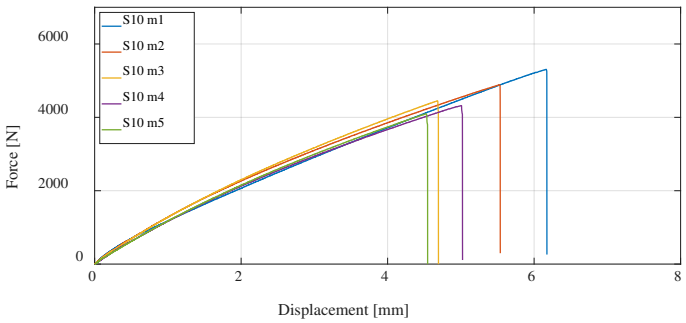

Figure 20. Displacement-force diagram for S10 experimental measurements.

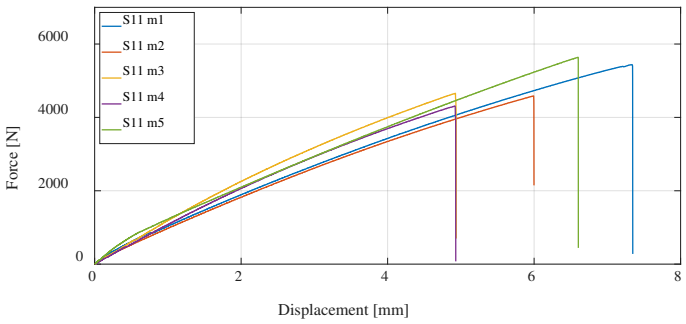

Figure 21. Displacement-force diagram for S11 experimental measurements.

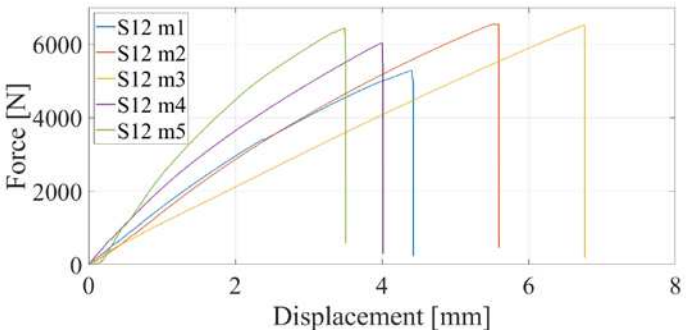

Figure 22. Displacement-force diagram for S12 experimental measurements.

Preprints (www.preprints.org) | NOT PEER-REVIEWED | Posted: 28 June 2023 doi:10.20944/preprints202306.1978.v1

As previously described, due to the problem of clamping composite materials into packs, increasing it to 16 layers makes clamping even more difficult. The higher the tensile strength of the specimen, the more difficult it is to clamp, that is, by increasing the fibers, the tensile strength significantly increases in the axial direction of the test specimen, but not so much in the radial direction of clamping, so the test specimens break due to excessive clamping. If it is not clamped enough, then slippage occurs, so there is a small range to clamp the test specimen so that it does not break, and on the other hand, so that it does not slip. Precisely because of these problems, only one sample out of 16 layers was tested. As expected, that sample had an even higher tensile strength. For this reason, in future work, testing on a different test device is planned.

4.2. Measurement Results Shown by Displacement-Force Diagrams

For a better presentation and visualization of the results, bar charts are used with the mean values of the maximum stress of each series of tested specimens. In the first diagram shown in Figure 23, the values of maximum stress for specimens S01 to S06 made of PLA and PETG materials using FDM process on the Prusa printer are compared. The diagram shown in Figure 24 shows specimens that actually represent the default parameters for three different technologies and three different printers. Therefore, specimens S01 (PLA) and S04 (PETG) which were produced using FDM, specimens S07, which were produced by the SLS from material PA 12, and finally, S08 produced by FDM technology using Onyx material. The following is a comparison of the maximum tensile strength of the composite materials that are the main focus of this research. Figure 25 shows all five series of specimens that were produced on the Onyx 3D printer, including the unreinforced specimens S08 to compare with the reinforced specimens.

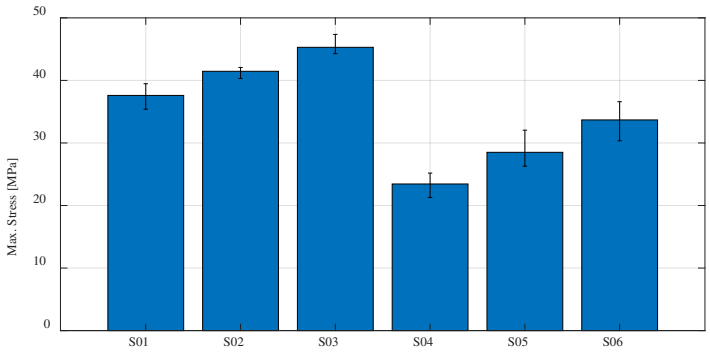

Figure 23. Mean values of the maximum stress regarding PLA and PETG materials.

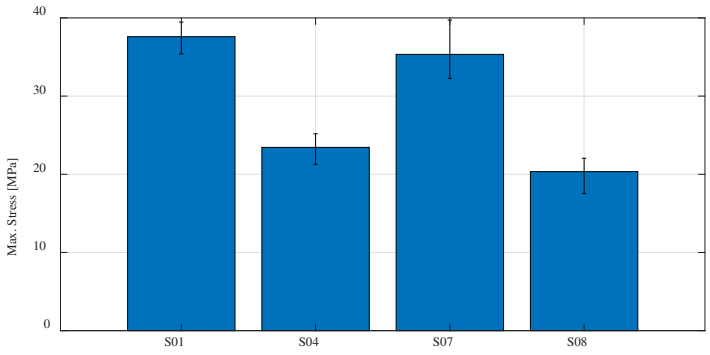

Figure 24. Mean values of the maximum stress regarding default print parameters for PLA, PETG, PA 12, and Onyx materials.

Preprints (www.preprints.org) | NOT PEER-REVIEWED | Posted: 28 June 2023 doi:10.20944/preprints202306.1978.v1

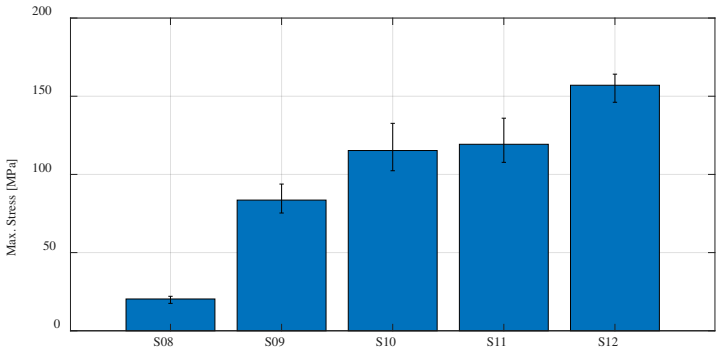

Figure 25. Mean values of the maximum stress regarding CFF technology using Onyx and fiberglass reinforcement.

Onyx material from which series 8 was produced, is further used as a matrix material for the production of specimens series (S09, S10, S11, and S12). Apart from the fact that the type of reinforcement (concentric or isotropic) and the orientation of the fibers affect the maximum stress, the number of layers in which the fibers are applied has the greatest influence. Considering that of the specimens (S09, S10, S11) which are reinforced with 8 layers of fibers, the sample S11 with the highest maximum tensile strength is further considered and the proportion of fibers is increased to 12. The specimens S12 with 12 fiber layers orientation is obtained $[30/45/60/0]_{12}$ which, as expected, gives the highest value of maximum tensile strength. With 12 layers of fibers, the tensile strength is up to 164.11 MPa. For one measurement that has been completed in case of 16 fibers, the tensile strength of 173.99 MPa was recorded.

5. Discussion and Conclusions

The choice of printing technology and material depends on the application of the structural part. In this paper, the focus was on CFF technology, which enables the production of parts of the airframe of multirotor UAVs that are mechanically loaded. Although different mechanical properties can be obtained by combining the proportion and orientation of the fibers as shown by the experiment, when making the structural part, it is also necessary to take into account the manufacturing costs. For early development and prototyping, it is most advantageous to use FDM technology due to the low cost and faster model creation if mechanical properties are not crucial when making the assembly and testing the part. Comparing the materials of FDM technology, regardless of the 3D printing parameters, PLA has a higher tensile strength compared to PETG material for the same printing parameters. The difference between the lowest and highest obtained tensile strength values for the tested materials is not as significant as when changing the technology. If higher tensile strength and stiffness of the structural airframe part are required, it is more advantageous to use CFF technology, because higher values are achieved compared to FDM and SLS AM technologies. The characterization of test samples produced by CFF technology with different reinforcement parameters was carried out in this research. First, tests were carried out on an unreinforced specimens (S08) made from micro carbon fiber-filled nylon Onyx material. The lowest values of tensile strength are obtained in relation to all considered technologies and materials in this research. However, the highest ductility is obtained for the same material as shown by experiments, which makes this material suitable as a matrix for composite connection applying fiberglass.

It has been shown by experiments that by using a default pattern of reinforced material, the mechanical properties are significantly improved with regard to tensile strength and ductility, which is the goal of obtaining optimal construction of UAVs. To further improve the mechanical properties of the material, it is necessary to change the orientation of the fibers. With the same number of layers of fiberglass, i.e. the volume fraction, they provide significantly better mechanical properties compared to the default values. Of the 3 tested orientations, $[0/90/\pm45]_8$ has the lowest maximum tensile strength and displacement, which still exceeds the tensile strength properties of some

aluminum alloys. By testing samples of 8 layers of different orientations, the highest value is obtained for sample $[30/45/60/0]_S$, which is below most aluminum alloys of the 5000 and 6000 series. In order to achieve higher tensile strength, comparable to mentioned aluminum alloys, a reinforcement pattern with the highest tensile strength in the case of 8 layers is chosen and tested on the case of 12 and 16 fiber layers. As shown in the literature, by increasing the proportion of fibers, the tensile strength also increases as shown for experimental testing.

Due to the similar requirements of the construction of UAVs to those of the automotive industry, such as absorption energy, lower mass, and high strength, the composites tested in this paper will be compared with aluminum alloys in future work.

Author Contributions: Conceptualization, T.Š. and D.K.; methodology, T.Š. and M.B.; software, D.K.; validation, T.Š. and M.B.; writing—original draft preparation, D.K.; writing—review and editing, A.L.; supervision, M.B. All authors have read and agreed to the published version of the manuscript.

Funding: This research was funded by European Regional Development Fund, Operational programme competitiveness and cohesion 2014–2020, grant number KK.01.1.1.04.0092 and the APC was funded by KK.01.1.1.04.0092.

Acknowledgments: This research was funded by European Regional Development Fund, Operational programme competitiveness and cohesion 2014–2020, grant number KK.01.1.1.04.0092.

Conflicts of Interest: The authors declare no conflict of interest.

References

1. Morgan, J.L.; Gergel, S.E.; Coops, N.C. Aerial Photography: A Rapidly Evolving Tool for Ecological Management. *BioScience* **2010**, *60*, 47–59. https://doi.org/10.1525/bio.2010.60.1.9
2. Yeom, S.; Cho, I.-J. Detection and Tracking of Moving Pedestrians with a Small Unmanned Aerial Vehicle. Appl. Sci. **2019**, 9, 3359. https://doi.org/10.3390/app9163359
3. Kim, J.; Kim,S.; Ju.C.; Son, H.I. Unmanned Aerial Vehicles in Agriculture: A Review of Perspective of Platform, Control, and Applications. *IEEE Access* **2019**, *7*, 105100-105115 . https://doi.org/10.1109/ACCESS.2019.2932119
4. Jannoura, R.; Brinkmann, K.; Uteau, D.; Bruns, C.; Joergensen, R.G. Monitoring of crop biomass using true colour aerial photographs taken from a remote controlled hexacopter. *Biosyst. Eng.* **2014**, *129*, 341-351. https://doi.org/10.1016/j.biosystemseng.2014.11.007
5. Villa, D.K.D.; Brandão, A.S.; Filho, M.S. A Survey on Load Transportation Using Multirotor UAVs. *J Intell Robot Syst* **2019**, *98*, 267–296. https://doi.org/10.1007/s10846-019-01088-w
6. Budholiya, S.; Bhat, A.; Raj, S.A.; Hameed Sultan, M.T.; Md Shah, A.U.; A. Basri, A. State of the Art Review about Bio-Inspired Design and Applications: An Aerospace Perspective. *Appl. Sci.* **2021**, *11*, 5054. https://doi.org/10.3390/app11115054
7. Puchalski, R.; Giernacki, W. UAV Fault Detection Methods, State-of-the-Art. *Drones* **2022**, *6*, 330. https://doi.org/10.3390/drones6110330
8. Carneiro, P.M.C.; Gamboa, P. Structural analysis of wing ribs obtained by additive manufacturing. *Rapid Prototyp. J.* **2019**, *25*, 708-720. https://doi.org/10.1108/RPJ-02-2018-0044
9. Kotarski, D.; Piljek, P.; Pranjić, M.; Grlj, C.G.; Kasać, J. A Modular Multirotor Unmanned Aerial Vehicle Design Approach for Development of an Engineering Education Platform. Sensors **2021**, 21, 2737. https://doi.org/10.3390/s21082737
10. Bortolini, M.; Galizia, F.G.; Mora, C. Reconfigurable manufacturing systems: Literature review and research trend. *J. Manuf. Syst.* **2018**, *49*, 93-106. https://doi.org/10.1016/j.jmsy.2018.09.005
11. Koren, Y. *The Global Manufacturing Revolution: Product-Process-Business Integration and Reconfigurable Systems*, 1st ed.; John Wiley & Sons, Inc. New York, NY, USA, 2010; ISBN:9780470618813.
12. Silveira, G.D.; Borenstein, D.; Fogliatto, F.S. Mass customization: Literature review and research directions. *Int. J. Prod. Econ.* **2001**, *72*, 1-13. https://doi.org/10.1016/S0925-5273(00)00079-7
13. Xiong, G.; Wang, F.Y.; Nyberg, T.R.; Shang, X.; Zhou, M.; Shen, Z.; Li, S.; Guo, C. From mind to products: towards social manufacturing and service. *IEEE/CAA J. Autom. Sin.* **2018,** 5, 47-57. https://doi.org/10.1109/JAS.2017.7510742
14. Kristiawan, R.B.; Imaduddin, F.; Ariawan, D.; Sabino, U.; Arifin, Z. A review on the fused deposition modeling (FDM) 3D printing: Filament processing, materials, and printing parameters. *Open Eng.* **2021**, *11*, 639-649. https://doi.org/10.1515/eng-2021-0063

15. Huang, J.; Qin, Q.; Wang, J. A Review of Stereolithography: Processes and Systems. Processes **2020**, 8, 1138. https://doi.org/10.3390/pr8091138
16. Kumar, S.; Selective laser sintering: A qualitative and objective approach. *JOM* **2003**, *55*, 43-47. https://doi.org/10.1007/s11837-003-0175-y
17. Patpatiya, P.; Chaudhary, K.; Shastri, A.; Sharma, S. A review on polyjet 3D printing of polymers and multi-material structures. *J. Mech. Eng. Sci.* **2022**, *236*, 7899-7926 . https://doi.org/10.1177/09544062221079506
18. Mekonnen, B.G.; Bright, G.; Walker, A. A Study on State of the Art Technology of Laminated Object Manufacturing (LOM). In: Mandal, D.K., Syan, C.S. (eds) CAD/CAM, Robotics and Factories of the Future. Lecture Notes in Mechanical Engineering. Springer, New Delhi. https://doi.org/10.1007/978-81-322-2740-3_21
19. Zohdi, N.; Yang, R. Material Anisotropy in Additively Manufactured Polymers and Polymer Composites: A Review. Polymers **2021**, 13, 3368. https://doi.org/10.3390/polym13193368
20. García-Domínguez, A.; Claver, J.; Camacho, A.M.; Sebastián, M.A. Considerations on the Applicability of Test Methods for Mechanical Characterization of Materials Manufactured by FDM. Materials **2020**, 13, 28. https://doi.org/10.3390/ma13010028
21. Mercado-Colmenero, J.M.; Rubio-Paramio, M.A.; la Rubia-Garcia, M.D.; Lozano-Arjona, D.; Martin-Doñate, C. A numerical and experimental study of the compression uniaxial properties of PLA manufactured with FDM technology based on product specifications. Int. J. Adv. Manuf. Technol. **2019**, *103*, 1893–1909. https://doi.org/10.1007/s00170-019-03626-0
22. Grodzki, W., Łukaszewicz, A. Design and manufacture of unmanned aerial vehicles (UAV) wing structure using composite materials. *Mater. Werkst.* **2015**, *46*, 269–278. https://doi.org/10.1002/mawe.201500351.
23. Basri, E.I.; Sultan, M.T.H.; Basri, A.A.; Mustapha, F.; Ahmad, K.A. Consideration of Lamination Structural Analysis in a Multi-Layered Composite and Failure Analysis on Wing Design Application. Materials **2021**, 14, 3705. https://doi.org/10.3390/ma14133705
24. Pratama, J.; Cahyono, S.I.; Suyitno, S.; Muflikhun, M.A.; Salim, U.A.; Mahardika, M.; Arifvianto, B. A Review on Reinforcement Methods for Polymeric Materials Processed Using Fused Filament Fabrication (FFF). Polymers **2021**, 13, 4022. https://doi.org/10.3390/polym13224022
25. Galatas, A.; Hassanin, H.; Zweiri, Y.; Seneviratne, L. Additive Manufactured Sandwich Composite/ABS Parts for Unmanned Aerial Vehicle Applications. Polymers **2018**, 10, 1262. https://doi.org/10.3390/polym10111262
26. Lupone, F.; Padovano, E.; Venezia, C.; Badini, C. Experimental Characterization and Modeling of 3D Printed Continuous Carbon Fibers Composites with Different Fiber Orientation Produced by FFF Process. Polymers **2022**, 14, 426. https://doi.org/10.3390/polym14030426
27. Espinoza-Fraire, T.; Saenz, A.; Salas, F.; Juarez, R.; Giernacki, W. Trajectory Tracking with Adaptive Robust Control for Quadrotor. *Appl. Sci.* **2021**, *11*, 8571. https://doi.org/10.3390/app11188571
28. Kotarski, D.; Piljek, P.; Pranjić, M.; Kasać, J. Concept of a Modular Multirotor Heavy Lift Unmanned Aerial Vehicle Platform. *Aerospace* **2023**, *10*, 528. https://doi.org/10.3390/aerospace10060528
29. Tiger Multirotor Motors Homepage. Available online: https://perma.cc/6ML9-LGK2 (accessed on 8 June 2023).
30. Łukaszewicz A., Panas K., Szczebiot R. Design process of technological line to vegetables packaging using CAx tools. Proceedings of 17th International Scientific Conference on Engineering for Rural Development, Jelgava, Latvia, 23-25 May 2018, pp. 871-87. https://doi.org/10.22616/ERDev2018.17.N494
31. Mircheski I., Łukaszewicz A., Szczebiot R. Injection process design for manufacturing of bicycle plastic bottle holder using CAx tools, Procedia Manuf. **2019**, *32*, 68 – 73. https://doi.org/10.1016/j.promfg.2019.02.184
32. Łukaszewicz, A., Szafran, K., Jóźwik, J. CAx techniques used in UAV design process, In Proceedings of the 2020 IEEE 7th International Workshop on Metrology for AeroSpace (MetroAeroSpace), Pisa, Italy, 22–24 June 2020; pp. 95–98. https://doi.org/10.1109/MetroAeroSpace48742.2020.9160091
33. Saleh Alghamdi, S.; John, S.; Roy Choudhury, N.; Dutta, N.K. Additive Manufacturing of Polymer Materials: Progress, Promise and Challenges. Polymers **2021**, 13, 753. https://doi.org/10.3390/polym13050753
34. Peyre. P.; Rouchausse, Y.; Defauchy, D.; Régnier, G. Experimental and numerical analysis of the selective laser sintering (SLS) of PA12 and PEKK semi-crystalline polymers. *J. Mater. Process. Technol.* **2015**, *225*, 326-336. https://doi.org/10.1016/j.jmatprotec.2015.04.030
35. Moghanizadeh, A. Development of 3D printing scaffolds by sacrificial ice support layers. *Manuf. Lett.* **2022**, *31*, 116-118. https://doi.org/10.1016/j.mfglet.2021.09.002
36. Nath, S.D.; Nilufar, S. An Overview of Additive Manufacturing of Polymers and Associated Composites. Polymers **2020**, 12, 2719. https://doi.org/10.3390/polym12112719
37. Patel, H.V.; Dave, H.K. Effect of fiber orientation on tensile strength of thin composites. *Mater. Today Proc.* **2021**, *46*, 8634-8638. https://doi.org/10.1016/j.matpr.2021.03.598

38. Zisopol, D.G.; Ion, N.; Portoaca, A.I. Comparison of the Charpy Resilience of Two 3D Printed Materials: A Study on the Impact Resistance of Plastic Parts. *Eng. Technol. Appl. Sci. Res.* **2023**, *13*, 10781–10784. https://doi.org/10.48084/etasr.5876
39. Brčić, M.; Kršćanski, S.; Brnić, J. Rotating Bending Fatigue Analysis of Printed Specimens from Assorted Polymer Materials. *Polymers* **2021**, *13*, 1020. https://doi.org/10.3390/polym13071020
40. N. Dickson, A.; Barry, J.N.; McDonnell, K.A.; Dowling, D.P. Fabrication of continuous carbon, glass and Kevlar fibre reinforced polymer composites using additive manufacturing. *Addit. Manuf.* **2017**, *16*, 146-152. https://doi.org/10.1016/j.addma.2017.06.004
41. Cordin, M.; Bechtold, T.; Pham, T. Effect of fibre orientation on the mechanical properties of polypropylene–lyocell composites. *Cellulose* **2018**, *25*, 7197–7210. https://doi.org/10.1007/s10570-018-2079-6
42. Shanmugam, V.; Johnson, R.D.J.; Babu NB, K.; Rajendran, S.; Veerasimman, A.; Marimuthu, U.; Singh, S.; Das, O.; Neisiany, R.E.; Hedenqvist, M.S.; Berto, F.; Ramakrishna, S. The mechanical testing and performance analysis of polymer-fibre composites prepared through the additive manufacturing. *Polym. Test.* **2021**, *93*, 106925. https://doi.org/10.1016/j.polymertesting.2020.106925
43. Parmiggiani, A.; Prato, M.; Pizzorni, M. Effect of the fiber orientation on the tensile and flexural behavior of continuous carbon fiber composites made via fused filament fabrication. *Int. J. Adv. Manuf. Technol.* **2021**, 114, 2085–2101. https://doi.org/10.1007/s00170-021-06997-5